nature neuroscience

ARTICLES

https://doi.org/10.1038/s41593-019-0342-2

Rapid, biphasic CRF neuronal responses encode positive and negative valence

Jineun Kim[1], Seongju Lee[1,6], Yi-Ya Fang[2,3,6], Anna Shin[1], Seahyung Park[1], Koichi Hashikawa[2,3], Shreelatha Bhat[1], Daesoo Kim[1], Jong-Woo Sohn[1], Dayu Lin[2,3]* and Greg S. B. Suh[1,2,4,5]*

Corticotropin-releasing factor (CRF) that is released from the paraventricular nucleus (PVN) of the hypothalamus is essential for mediating stress response by activating the hypothalamic–pituitary–adrenal axis. CRF-releasing PVN neurons receive inputs from multiple brain regions that convey stressful events, but their neuronal dynamics on the timescale of behavior remain unknown. Here, our recordings of PVN CRF neuronal activity in freely behaving mice revealed that CRF neurons are activated immediately by a range of aversive stimuli. By contrast, CRF neuronal activity starts to drop within a second of exposure to appetitive stimuli. Optogenetic activation or inhibition of PVN CRF neurons was sufficient to induce a conditioned place aversion or preference, respectively. Furthermore, conditioned place aversion or preference induced by natural stimuli was significantly decreased by manipulating PVN CRF neuronal activity. Together, these findings suggest that the rapid, biphasic responses of PVN CRF neurons encode the positive and negative valences of stimuli.

While animals encounter a wide range of environmental stimuli, they need to determine quickly whether the stimuli are beneficial or detrimental to their survival and whether they should be approached or avoided. How is sensory information of opposing valences represented and evaluated in the brain to produce discrete behavioral outputs? Previous studies have suggested that a key strategy in encoding opposing valences involves topologically segregated populations of neurons within a particular region of the brain[1,2]. An alternative strategy has been proposed, however, that only a single population of neurons is required to encode opposing valence. Specifically, it has been proposed that the activity of dopaminergic neurons that is stimulated by rewarding stimuli and inhibited by aversive cues[3] plays a key role in mediating opposing behaviors[4,5]. However, the extent to which the brain utilizes different encoding strategies to enhance survival and reproduction in the wild is not yet understood.

A population of neuroendocrine neurons in the PVN of the hypothalamus secretes CRF into the circulation during exposure to a stressor[6,7]. CRF, in turn, triggers the release of adrenocorticotropic hormone from the anterior pituitary gland to induce the secretion of glucocorticoids from the adrenal cortex, which comprises the final effector along the hypothalamic-pituitary-adrenal (HPA) axis[6,7]. This gradual two-step hormonal mechanism of HPA activation adjusts the neuroendocrine responses to stress. It does not, however, explain how PVN CRF neurons might be involved in rapid behavioral changes that occur in response to acute stress. Furthermore, how the activity of PVN CRF neurons is modulated by a diverse array of stressful stimuli and how they differ from the responses to neutral and appetitive environmental stimuli remain unclear. These issues have been difficult to address largely because CRF neuronal responses were investigated using immediate early gene mapping, which has a temporal resolution of minutes to hours and is unable to effectively measure a reduction in neuronal activity.

To understand the response of PVN CRF neurons to acute environmental stimuli in awake, freely behaving animals, we used fiber photometry[8,9], an in vivo calcium imaging technique that measures the total fluorescence of a calcium reporter expressed in a population of neurons. Calcium imaging experiments revealed that PVN CRF neurons are immediately activated by all aversive cues tested thus far and are rapidly suppressed by appetitive stimuli. Furthermore, optogenetic manipulation of PVN CRF neuronal activity was sufficient to induce conditioned aversion or preference towards the initially neutral context in a real-time place avoidance (RTPA) or preference (RTPP) assay. Notably, these manipulations also overrode aversion or preference to natural aversive or appetitive stimuli.

Results

Rapid increase in PVN CRF neuronal activity by aversive stimuli. We virally expressed a Cre-dependent GCaMP6s calcium indicator in CRF-ires-Cre mice, and recorded changes in GCaMP6s fluorescence signal through a 400-μm optic fiber placed above the PVN (Fig. 1a). The resulting trace represents the integrated activity of PVN CRF neurons. Histological analysis revealed that over 95% of GCaMP6-expressing cells overlap with CRF-positive cells in the PVN in mice that were used for calcium imaging experiments (Fig. 1a).

We first investigated changes in GCaMP6 fluorescence intensity in PVN-CRF^{GCaMP6} mice that were subjected to various stress-inducing conditions. During a forced swim test (FST), which increases c-Fos expression in PVN CRF neurons significantly[10], in vivo recordings revealed a substantial increase in GCaMP intensity when the mice were captured and then dropped into the water, which rose continuously until the mice were removed from the water (Fig. 1b,c). The GCaMP intensity remained high when the mice were returned to their home cage but gradually returned to pretest baseline levels over 20 minutes (Fig. 1c). During tail-restraint test (TRT), we also observed a rapid increase in GCaMP intensity in PVN CRF

[1]Department of Biological Sciences, Korea Advanced Institute of Science and Technology, Daejeon, Republic of Korea. [2]Neuroscience Institute, New York University School of Medicine, New York, NY, USA. [3]Department of Psychiatry, New York University School of Medicine, New York, NY, USA. [4]Skirball Institute of Biomolecular Medicine, New York University School of Medicine, New York, NY, USA. [5]Department of Cell Biology, New York University School of Medicine, New York, NY, USA. [6]These authors contributed equally: S. Lee, Y.-Y. Fang. *e-mail: Dayu.Lin@nyulangone.org; Gregsuh@gmail.com; Greg.suh@med.nyu.edu

neurons when mice were chased and lifted by hand (Fig. 1d,e and Supplementary Fig. 1a,e). After several rounds of TRTs, the baseline GCaMP fluorescence gradually increased (Fig. 1d). Control mice with PVN CRF neurons expressing GFP showed little or no change in fluorescent intensity during these stress-inducing conditions, suggesting that the observed changes in $\Delta F/F$ were not movement artifacts (Supplementary Fig. 2).

PVN CRF neuronal activity also increased in mice exposed to other exteroceptive stressors, such as a looming stimulus or predator odor. The looming stimulus consisted of a pigeon-sized object moving above the mice to mimic a flying predator. This triggered bursts of defensive responses such as flight and freezing in mice (Fig. 1f,g and Supplementary Fig. 1b,f). These signals did not increase significantly, however, when the object was 'flying' lateral to the mice (Supplementary Fig. 3a). To investigate this effect further, we compared the response of PVN CRF neurons when the mice were exposed to an expanding, looming disk, which simulates a rapidly approaching object above, along the side or below a transparent cage in which the mice were placed. The looming disk above the cage, which triggered robust defensive behavior in mice[11], resulted in the strongest activation of PVN CRF neurons (Fig. 1f,g, Supplementary Fig. 3b, and Supplementary Video 1). Notably, GCaMP signals started to rise before the onset of flight or freezing (Fig. 1f, f' and Supplementary Fig. 1d,h).

Aversive olfactory stimuli also stimulated the activity of PVN CRF neurons. Exposure to a predator odor, 2,3,5-trimethyl-3-thiazoline (TMT), mostly triggered freezing responses in mice[12]. We found a significant increase in GCaMP signals in these neurons before the mice displayed the onset of defensive response (Fig. 1h,i). Thus, aversive stimuli of different sensory modalities rapidly stimulated the activity of PVN CRF neurons (Fig. 1j).

In addition to exteroceptive stressors, we tested whether an interoceptive stressor could activate PVN CRF neurons and found that intraperitoneal injection of lithium chloride (LiCl), a reagent that causes gastric malaise, significantly increased the intensity of GCaMP6 fluorescence in CRF neurons compared with saline injection (Fig. 1k–m).

We next investigated the response of PVN CRF neurons when the mice were subjected to another type of interoceptive stressor, food deprivation. Following 22 hours of food deprivation, the baseline calcium levels and calcium transients in PVN CRF neurons were increased compared with those in refed animals (Supplementary Fig. 4a,b and also see Fig. 2). This is consistent with the increased c-Fos expression detected in PVN CRF neurons during prolonged periods of food deprivation (Supplementary Fig. 4c,d). These findings further support the view that PVN CRF neurons respond to a wide range of aversive stimuli.

Suppression of PVN CRF neuronal activity by appetitive stimuli. While it is unanticipated that aversive stimuli rapidly stimulated the activity of PVN CRF neurons, their role in activating the HPA axis has been established through previous c-Fos studies[10]. It is completely unknown, however, whether PVN CRF neurons respond to appetitive stimuli. To investigate the response of these neurons to such stimuli, we measured changes in GCaMP intensity in PVN CRF neurons in response to food (see Supplementary Video 2). We first introduced a control pellet-sized neutral object into the home cage for 15 minutes, followed by a normal food chow pellet for 25 minutes (Fig. 2a). While the control object caused no significant change, the intensity of GCaMP signal in these neurons decreased significantly when the chow pellet was introduced (Fig. 2a–c). The decrease was more precipitous and pronounced in fasted mice than in fed mice, but was significant in fed mice. Intriguingly, GCaMP signals started to drop even before the mice took their first bite of food (Fig. 2c and also see Fig. 2j).

To determine whether the sensory cue of food is sufficient to reduce the activity of PVN CRF neurons, we provided a chow pellet or highly palatable peanut butter in a mesh-covered cup to prevent physical contact with it while allowing the mice to see it and smell it (Fig. 2d,g). In these mice, GCaMP signals were significantly suppressed initially, but soon increased to higher levels (Fig. 2d,f,g,i). The kinetics of the initial GCaMP suppression in these mice were indistinguishable from those in mice freely consuming chow pellets or peanut butter (Fig. 2k–l). GCaMP signals further dropped when the mice had their first bite of food; a larger decrease was observed in fasted mice than in fed mice (Fig. 2d,e,g,h,j). Notably, PVN CRF neuronal activity remained suppressed between feeding bouts (Fig. 2a,d,g) or was not suppressed further by additional food

Fig. 1 | Rapid increase in PVN CRF neuronal activity by aversive stimuli. a, Viral construct and implantation scheme for fiber photometry on PVN CRF neurons. Middle: a representative image validates GCaMP6s expression in CRF neurons and optical fiber tract above the PVN. Scale bar, 100 µm. Further right: images depict the overlap between GCaMP6s-expressing cells (green) and anti-CRF-positive cells (red). Scale bar, 20 µm. Right: bar graph showing the percentage of GCaMP6s$^+$ neurons co-expressing CRF ($N=4$ mice). **b**, Schematic for FST and a representative trace illustrating an increase of PVN-CRF^{GCaMP6} signal during FST (red bar, above) and decreasing activity while back in home cage (white bar). Behavioral epochs, swimming (light blue) and climbing (blue), annotated in color-coded shaded bars. **c**, Plot (left) and heat map (right) across animals aligned to the start and end of FST, and the following rest in home cage. Black bold line and gray shadow in this and following figures indicate mean and s.e.m., respectively ($N=6$ mice). **d**, Schematic for TRT and a representative trace showing increases of PVN-CRF^{GCaMP6} signal during restraint (red bars, above). Color-coded shaded bars depict the periods during which mice were chased by a hand (gray) and struggled (beige). **e**, PETH plot (left) and heat map (right) across animals aligned to the start of TRT ($N=7$ mice). **f**, Schematic for presenting an overhead object and a representative trace showing increases of PVN-CRF^{GCaMP6} signal during the presentations (red bars, above). Shaded bars depict the epochs during which mice exhibited flight (red) and freezing (beige). **g**, PETH plot (left) and heat map (right) across animals aligned to the onset of overhead presentation ($N=7$ mice). **f'**, Schematic for a looming shadow disk and a representative trace showing increases of PVN-CRF^{GCaMP6} signal during the presentations (red bars, above). Shaded bars depict the epochs during which mice exhibited flight (red), freezing (beige) and hiding in a nest (yellow). **g'**, PETH plot (left) and heat map (right) across animals aligned to the onset of looming presentation ($N=8$ mice). **h**, Schematic of odor presentation and a representative trace showing increases of PVN-CRF^{GCaMP6} signal during TMT exposure (red bar, above). Shaded bar depicts the epoch during which mice exhibited freezing (beige). **i**, Plot across animals aligned to the start and end of TMT exposure ($N=6$ mice); 6 of 9 mice that displayed a defensive response showed an increase in GCaMP signal. **j**, Comparison of average $\Delta F/F$ of PVN-CRF^{GCaMP6} in response to different aversive stimuli. The measurements shown in blue dots are illustrated in the representative traces in **b**, **d**, **f**, and **h**. **k**, Schematic of intraperitoneal (i.p.) administration under anesthesia and a representative trace showing increases of PVN-CRF^{GCaMP6} signal after injection of LiCl. Shaded bars depict the period during which a mouse was placed in an anesthesia chamber (gray) and the period during which the mouse received LiCl injection (red). **l**, Plot across animals before and 30 min after LiCl injection (black line) and saline (gray line) ($N=8$ mice). Arrow head depicts the increase in GCaMP signal. **m**, Bar graphs showing average $\Delta F/F$ of PVN-CRF^{GCaMP6} for 30 min after injection of LiCl or saline. The measurement shown in a blue dot is illustrated in the representative traces in **k**. Paired two-tailed t-test for GCaMP signal before versus during exposure. $^*P<0.05$, $^{**}P<0.01$, $^{***}P<0.001$. Data are presented as mean ± s.e.m. See Supplementary Table 1 for detailed description of statistics for this figure and subsequent figures. 3V, third ventricle; LV, lateral ventricle.

consumption (Supplementary Fig. 5). These results suggest that GCaMP signals are not correlated with individual feeding bouts, but instead with the reward value of food, which is determined by the palatability of food and the nutritional state of animals. The overall frequency of calcium transients in PVN CRF neurons was significantly suppressed after animals consumed food; the suppression was more substantial in fasted mice than in fed mice (Supplementary Fig. 6a,b and also see Fig. 2a,d,g).

PVN CRF neuronal responses during social interaction. We next sought to investigate the activity of PVN CRF neurons in response to social stimuli. We introduced a pup or a CD1 aggressor[13] into the home cage of a mouse in which GCaMP activity in PVN CRF neurons was continuously recorded. In a female mouse, PVN CRF neuronal activity was robustly and rapidly suppressed after a pup was introduced to her cage (Fig. 3a). Similar to the acute PVN CRF neuronal response to food, GCaMP signals began to drop as soon

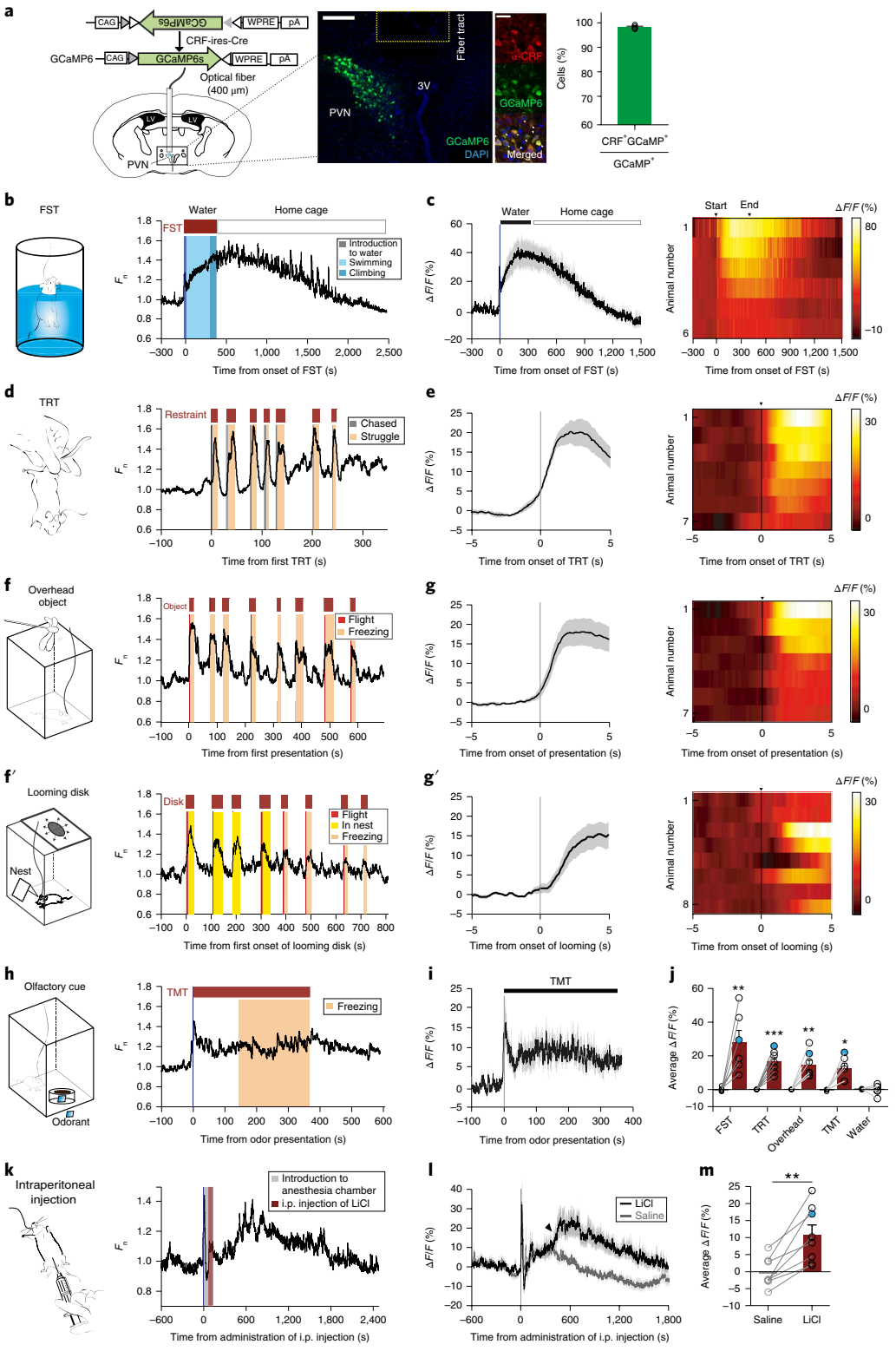

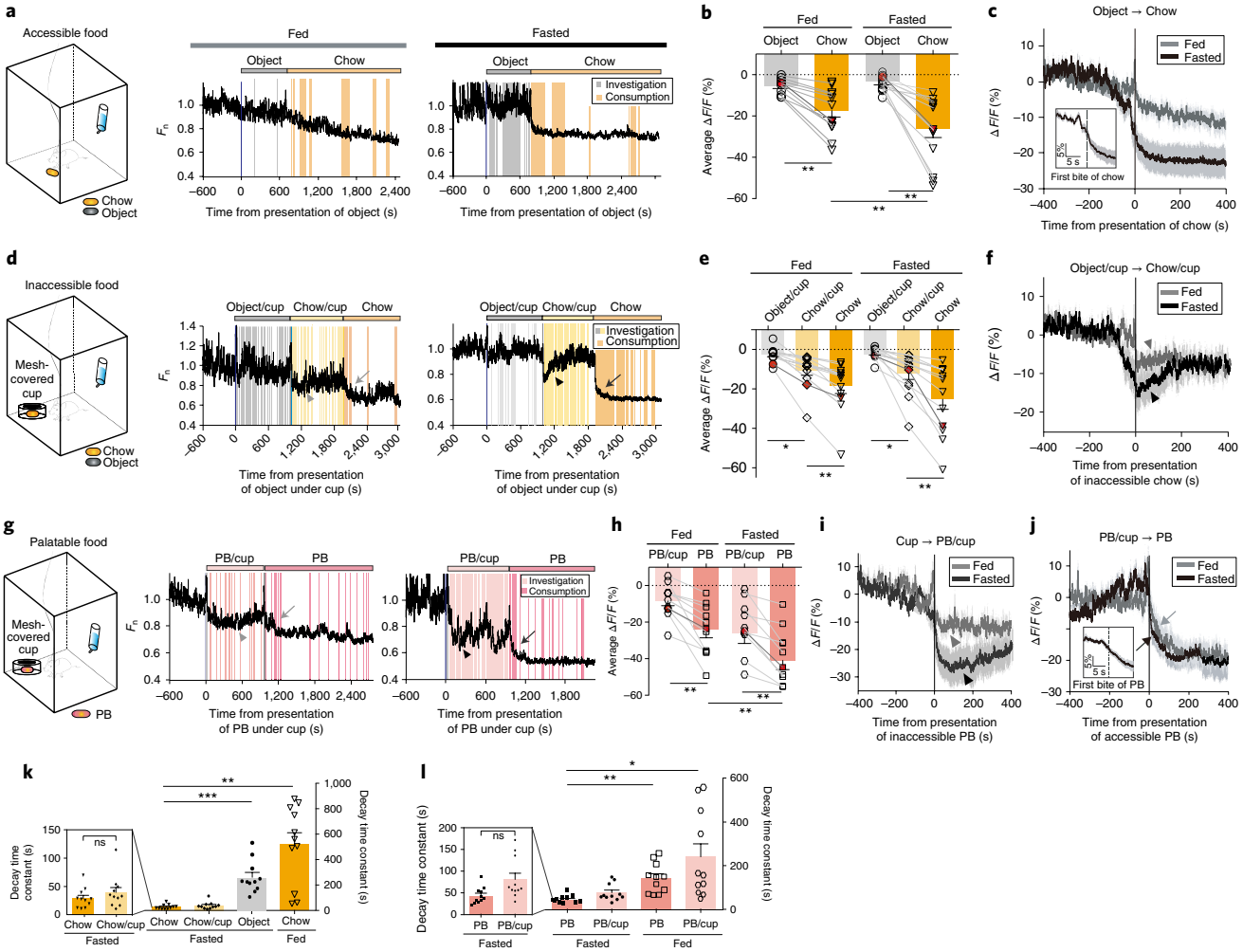

Fig. 2 | Suppression of PVN CRF neuronal activity by appetitive cues. a, Schematic for freely accessible chow presentation in a chamber and representative traces showing PVN-CRF^{GCaMP6} signal. Ad libitum fed or 22-h fasted mice were freely exposed to a non-food object (gray bar), followed by chow pellet (orange bar). Shaded bars depict the epochs during which mice investigated the non-food object (gray) and consumed the chow pellet (orange). **b**, Bar graph summarizing average $\Delta F/F$ of PVN-CRF^{GCaMP6} when exposed to a non-food object or chow pellet. The measurements shown in red dots are illustrated in the representative traces in **a**. **c**, Plot across animals aligned to the introduction of chow ($N = 11$ mice). Inset: PETH plot across animals, aligned to the first bite of chow pellet. **d**, Schematic for inaccessible chow presentation in a chamber and representative traces showing PVN-CRF^{GCaMP6} signal. Ad libitum fed or 22-h fasted mice were exposed to a non-food object (gray bar) and then to a chow pellet in a mesh-covered cup (yellow bar) followed by an accessible chow pellet (orange bar). Shaded bars depict the epochs during which mice investigated the non-food object (gray) or the chow in a mesh-covered cup (yellow) and during which they consumed the chow pellet (orange). 'Chow/cup' indicates that chow was present but inaccessible. Arrowheads depict a drop in PVN-CRF^{GCaMP6} signal when mice inspected a chow pellet in a mesh-covered cup. Arrows indicate a drop in PVN-CRF^{GCaMP6} signal when a mouse consumed a chow pellet. **e**, Bar graph summarizing average $\Delta F/F$ of PVN-CRF^{GCaMP6} when exposed to a non-food object or chow in a mesh-covered cup and when exposed to an accessible chow pellet. The measurements shown in red dots are illustrated in the representative traces in **d**. **f**, Plot across animals aligned to the introduction of inaccessible chow in a mesh-covered cup ($N = 11$ mice). **g**, Schematic for the presentation of inaccessible peanut butter (PB) followed by accessible PB in a chamber, and representative traces showing PVN-CRF^{GCaMP6} signal. Ad libitum fed or 22-h fasted mice were exposed to PB in a mesh-covered cup (light pink bar) followed by freely accessible PB (pink bar). Shaded bars depict the epochs during which mice investigated PB in a mesh-covered cup (light pink) and consumed PB (pink). 'PB/cup' indicates that peanut butter was present but inaccessible. Arrowheads depict a drop in PVN-CRF^{GCaMP6} signal when mice inspected PB in a mesh-covered cup. Arrow indicates a drop in PVN-CRF^{GCaMP6} signal when a mouse consumed PB. **h**, Bar graph summarizing average $\Delta F/F$ of PVN-CRF^{GCaMP6} when exposed to PB in a mesh-covered cup and accessible PB. The measurements shown in red dots are illustrated in the representative traces in **g**. **i**, Plot across animals aligned to the introduction of inaccessible PB in a mesh-covered cup ($N = 11$ mice). **j**, Plot across animals aligned to the introduction of PB ($N = 11$ mice). Inset: PETH plot across animals, aligned to the first bite of PB. **k**,**l**, Bar graph illustrating the decay time constant, the time at which GCaMP6 signal reaches 63.2% of the maximal change from the onset (see also Methods), when exposed to accessible non-food object and a chow pellet, when exposed to an inaccessible chow pellet in a mesh-covered cup (**k**), and when exposed to PB and inaccessible PB in a mesh-covered cup. **l**, Left graph magnifies the two bars representing accessible chow and inaccessible chow (**k**), and accessible PB and inaccessible PB (**l**). One-way ANOVA test with Holm–Sidak post hoc analysis. $^*P < 0.05$, $^{**}P < 0.01$, $^{***}P < 0.001$. Data are presented as mean ± s.e.m.

as the female mouse oriented and approached towards the introduced pup (Fig. 3a,b,d and Supplementary Fig. 7a). The GCaMP signal continued to drop at the onset of close interactions such as sniffing, grooming, and crouching over the pup (Fig. 3a,d and Supplementary Fig. 7b). Notably, the GCaMP signal did not drop further when she approached or interacted with the pup from the

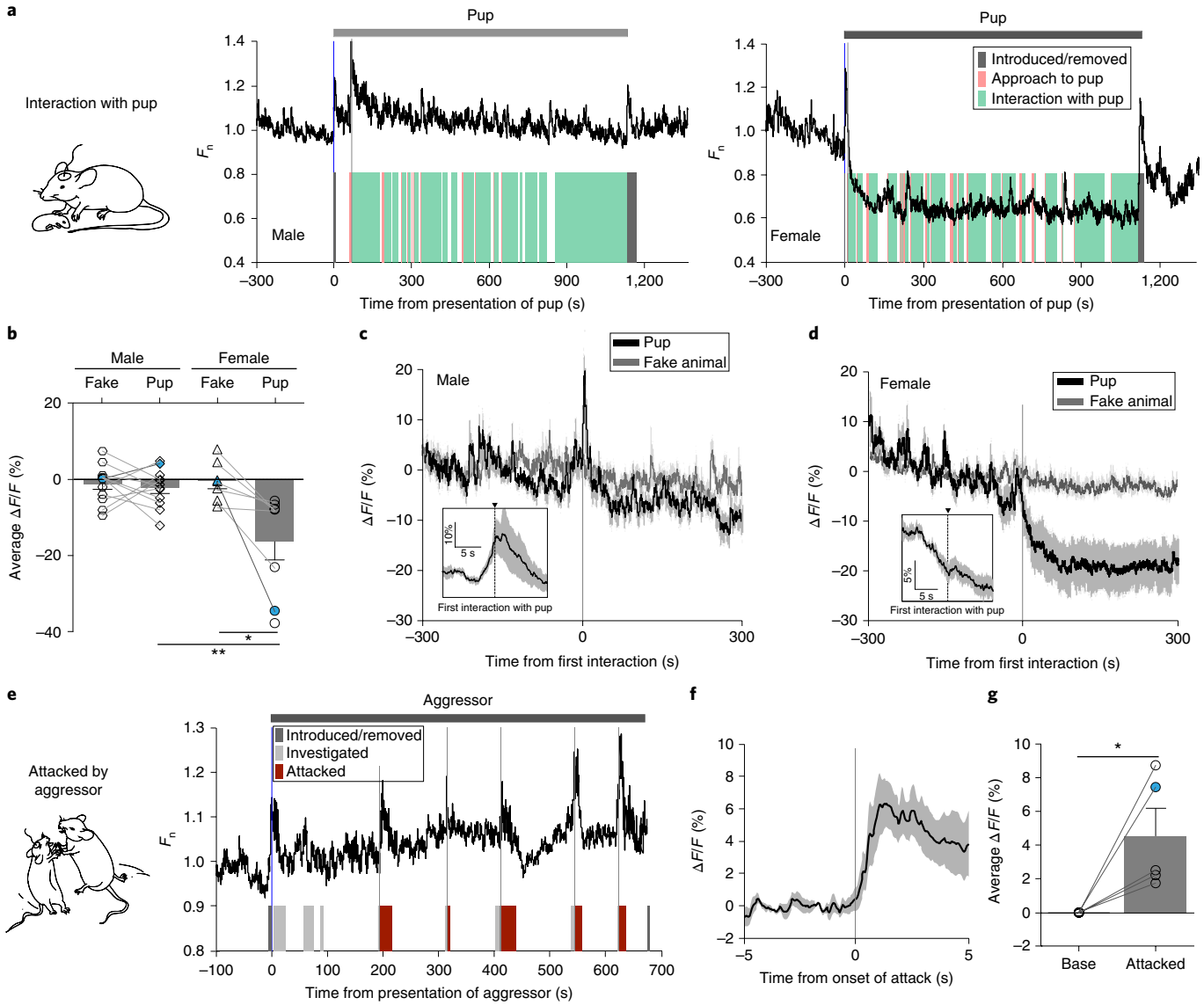

Fig. 3 | PVN CRF neuronal responses during social interaction. a, Schematic for interaction with pup and representative traces illustrating PVN-CRF^{GCaMP6} signal in a male (left) or a female (right) during the presence of a pup. Shaded bars depict the epochs during which the recorded mouse approached a pup (orange) and interacted with the pup (green) and during which the pup was introduced or removed from the arena (gray). **b**, Bar graph summarizing average $\Delta F/F$ of PVN-CRF^{GCaMP6} during the presence of a pup or a fake animal ($N=12$ males; $N=7$ or 8 females). The measurements shown in blue dots are illustrated in the representative traces in **a**. **c**,**d**, PETH plot across male mice ($N=12$) (**c**) and across female mice ($N=8$) (**d**) aligned to the onset of first interaction with pups. Insets: plot across animals aligned to the onset of first interaction with pup in a 10-s time window. **e**, Schematic for mouse being attacked by aggressor and a representative trace illustrating acute surge in PVN-CRF^{GCaMP6} signal at the onset of being investigated (light gray) or being attacked (red) by the male aggressor and when being introduced or removed from the arena (gray). **f**, PETH plot across animals aligned to the onset of attack by male mice ($N=5$). **g**, Bar graph summarizing average $\Delta F/F$ of PVN-CRF^{GCaMP6} during attack. The measurement shown in a red dot is illustrated in the representative traces in **e**. Mann–Whitney two-tailed *U*-test in **b** (male versus female); Wilcoxon two-tailed matched signed-rank test in **b** (fake versus pup in female); and paired two-tailed *t*-test in **g** (base versus attacked) were used. $^*P<0.05$, $^{**}P<0.01$. Data are presented as mean ± s.e.m.

second time and onwards (Supplementary Fig. 7a,b). By contrast, when a female mouse was presented with a fake animal, the activity of PVN CRF neurons did not change (Fig. 3b,d and Supplementary Fig. 7c–e). Similar to the suppressed PVN CRF neuronal activity during the presence of food, GCaMP signals remained suppressed during the entire period when female mice were exposed to pups (Fig. 3a,d). Likewise, the calcium transients in PVN CRF neurons of female mice were substantially reduced during the presentation of pups (Supplementary Fig. 6c,d).

In male mice, however, PVN CRF neuronal activity surged when a pup was introduced to their home cage, but soon decreased to the original baseline and remained unaltered during the presence of pups (Fig. 3a,c and Supplementary Fig. 7a,b). The calcium transients also remained unchanged (Supplementary Fig. 6c,d). Male mice did investigate the pups such as sniffing, but rarely exhibited grooming or crouching, as observed in female mice (data not shown). These findings indicate that a pup is perceived to be attractive to female mice, but not necessarily to male mice. Previous studies have demonstrated that a pup can be presented as positive reinforcement to virgin female rodents in a place conditioning task[14].

When a recorded male or female mouse was attacked by an aggressive CD1 intruder—a male or a lactating female, we observed

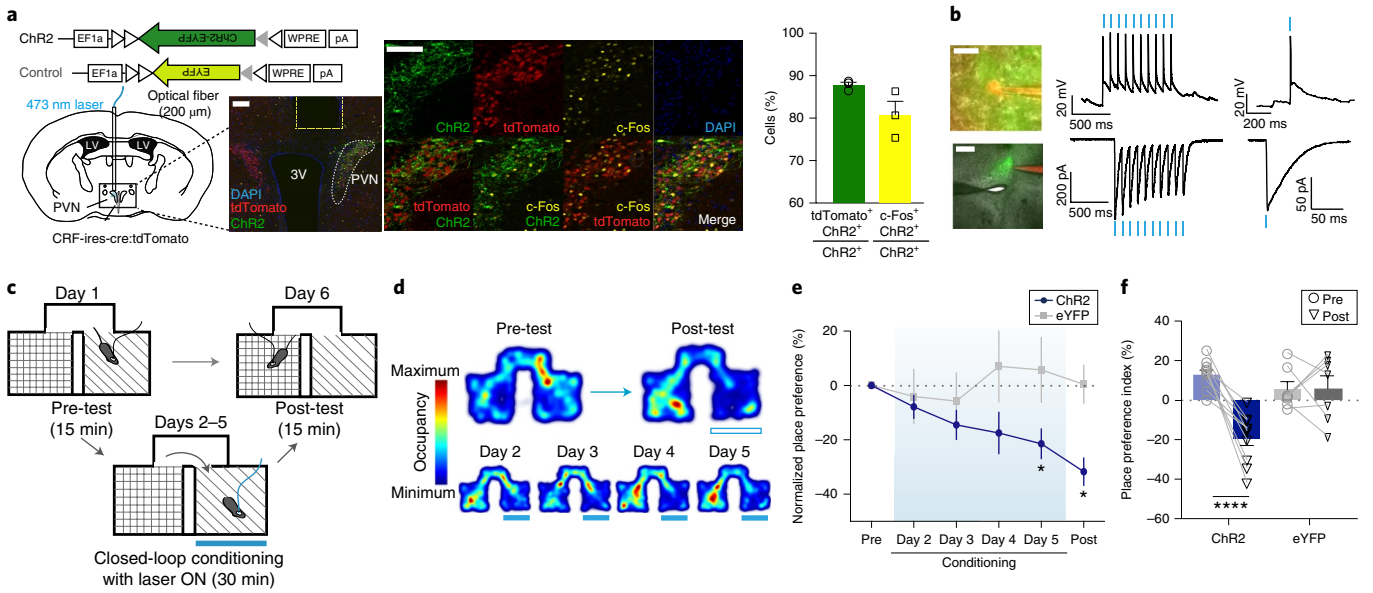

Fig. 4 | Optogenetic activation of PVN CRF neuronal activity induces CPA. a, Left: viral construct and schematic for unilateral injections of ChR2 and fiber implantation for optogenetic activation of PVN CRF neurons. Representative image illustrating the fiber tract above the PVN. Scale bar, 100 μm. Middle: representative images showing ChR2-EYFP-expressing cells (green), tdTomato-positive cells (red), c-Fos-expressing cells (yellow), and DAPI (blue). Nearly all CRF^{+} cells in the PVN of CRF-ires-cre (Jackson Stock no. 012704)-carrying Ai14 (Jackson Stock No: 007914) mice are tdTomato^{+} cells[10,32]. Scale bar, 100 μm. Right: bar graphs showing the percentages of ChR-EYFP^{+} cells co-expressing tdTomato or c-Fos ($N = 4$ mice). **b**, Ex vivo whole-cell patch-clamp recording of a representative PVN-CRF^{ChR2} cell showing optogenetic activation. Left: image of a recorded PVN-CRF^{ChR2} cell. ChR2-EYFP (green), Alexa Fluor 594 (red), 60× magnification (upper: scale bar, 20 μm) and 5× magnification (lower: scale bar, 200 μm). Middle: response of a PVN-CRF^{ChR2} cell to a train of light pulses (10 Hz, 10 ms pulse width, blue bars) for 1 s in current clamp (upper) and voltage clamp (lower) mode. Right: response of a PVN-CRF^{ChR2} cell to a pulse of blue light (3 ms, blue bar) in current clamp mode (upper) and voltage clamp mode (lower). Similar responses were observed in all five other recorded cells. **c**, Schematic of RTPA experiment. Closed-loop photostimulation was delivered on conditioning days. **d**, Representative locomotor traces from a PVN-CRF^{ChR2} mouse that received photostimulation at 473 nm (blue bars) before and after conditioning (upper) and after each day of conditioning (bottom). **e**, Normalized place preference index (%) for the photostimulation-paired side: average preference indices of PVN-CRF^{ChR2} mice (blue) and control PVN-CRF^{eYFP} mice (gray). **f**, Raw individual place preference indices (%) of PVN-CRF^{ChR2} ($N = 10$, blue) and PVN-CRF^{eYFP} ($N = 7$, gray) mice before and after conditioning. The photostimulation-paired chamber is chosen based on the mouse's initial preference to the chamber. Two-way ANOVA test with Holm–Sidak post hoc analysis. $^{*}P < 0.05$, $^{****}P < 0.0001$. Data are presented as mean ± s.e.m.

a rapid and dramatic increase in GCaMP signal in PVN CRF neurons during the attack (Fig. 3e–g and Supplementary Fig. 8). After being attacked repeatedly, the GCaMP activity stayed elevated (Fig. 3e and Supplementary Fig. 8). When male-intruder interactions did not involve aggression, we did not observe noticeable changes in PVN CRF neuronal activity (Supplementary Fig. 9).

Optogenetic activation or inhibition of PVN CRF neuronal activity induces conditioned place aversion (CPA) or preference (CPP). The rapid and bidirectional changes in PVN CRF neuronal activity suggest that these neurons communicate real-time information about the positive and negative valence of the encountered stimuli. To examine whether there is a causal relationship between the activity of PVN CRF neurons and behavior, we tested whether manipulating PVN CRF neuronal activity was sufficient to confer aversive or attractive response. To this end, we unilaterally injected a Cre-dependent AAV Channelrhodopsin-2 (ChR2) fused to eYFP (AAV-DIO-ChR2-eYFP)[15,16] or a control virus carrying eYFP alone into the PVN of CRF-ires-Cre mice carrying Rosa-lox-STOP-lox-tdTomato (Ai14) (Fig. 4a). We confirmed ChR2 expression by colabeling of the Cre-dependent eYFP reporter with tdTomato fluorescence in PVN CRF neurons (Fig. 4a). We validated blue light-evoked activation and spiking of PVN CRF neurons in vivo through c-Fos induction (Fig. 4a) and through whole-cell patch clamp recordings from the brain slices (Fig. 4b).

Following verification of the functional activation of PVN CRF neurons and observing the stereotypic display of grooming induced by photostimulation of PVN CRF neurons as previously reported[17], we asked whether artificial activation of PVN CRF neurons (473 nm, 10 ms, 10 Hz, maximally 30 seconds with 1 minute of interval) could serve as an unconditioned stimulus for the formation of aversive memories. To do this, we subjected mice that had received injections of AAV-DIO-ChR2-eYFP or AAV-DIO-eYFP to a closed-loop RTPA assay[18], where a mouse freely explored 2 chambers, 1 in which the mouse received photostimulation of PVN CRF neurons for 30 minutes for 4 days (Fig. 4c). We found that 4 days of conditioning resulted in the development of CPA in mice expressing ChR2 in PVN CRF neurons, but not in control mice (Fig. 4d–f).

To investigate whether inhibition of PVN CRF neuronal activity can induce preference, we tested mice (CRF-ires-Cre:Ai14) that had received bilateral injections of a Cre-dependent AAV-eArch3.0 fused to eYFP (AAV-DIO-eArch3.0-eYFP)[19,20] or the control AAV-DIO-eYFP in a similar RTPP assay (Fig. 5a). We confirmed the expression of eArch3.0-eYFP in PVN CRF neurons by colabeling it with tdTomato in these mice (Fig. 5a). We verified that green light evoked inhibition of PVN CRF neuronal activity measured by whole-cell patch clamp recordings of eArch3.0-expressing CRF neurons (Fig. 5b).

Similar to the RTPA experiment, a mouse received continuous green light (532 nm) that inhibited PVN CRF neuronal activity whenever it entered 1 of the freely exploratory 2 chambers during 30 minutes of conditioning on each day (Fig. 5c). Photoinhibition of PVN CRF neurons robustly promoted CPP towards the paired context (Fig. 5d–f). Strikingly, on the first day of conditioning, these

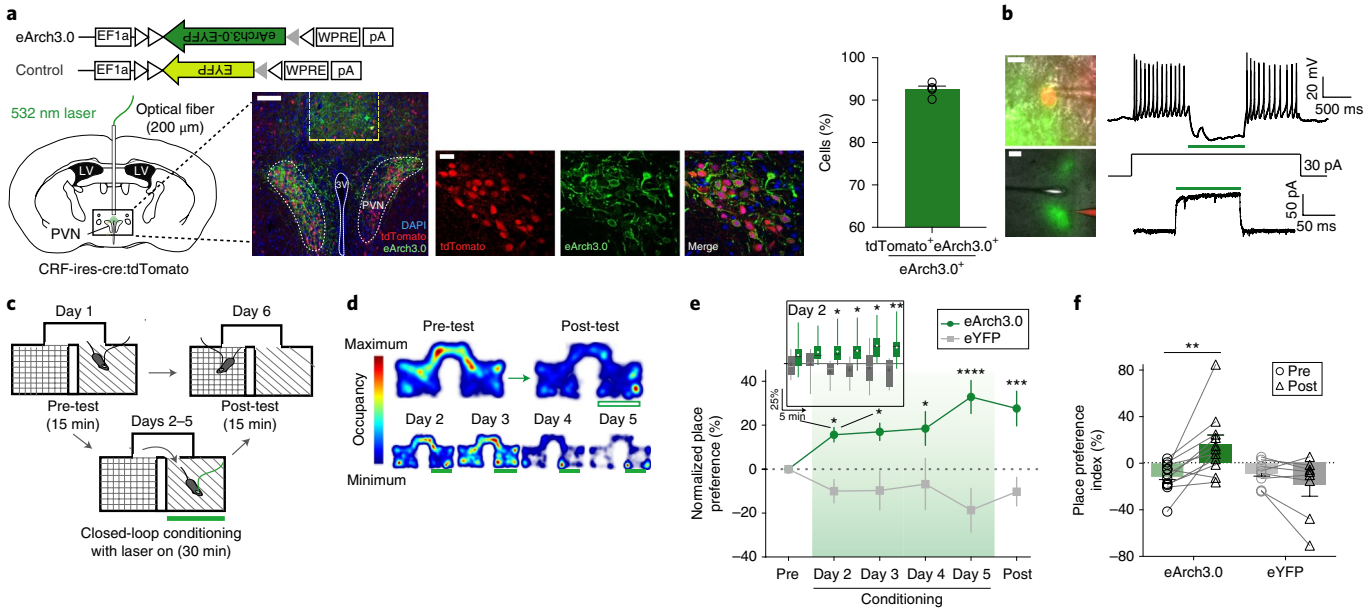

Fig. 5 | Optogenetic inhibition of PVN CRF neuronal activity drives CPP. a, Left: schematic illustrating bilateral vial injections for eArch3.0 and fiber implantation for optogenetic inhibition of PVN CRF neurons. Representative image illustrating the fiber tract above the PVN (scale bar, 100 μm). Middle: representative images showing the overlay of eArch3.0-expressing cells (green) and tdTomato-positive cells (red). Nearly all CRF^{+} cells in the PVN of CRF-ires-cre:Ai14 mice are tdTomato^{+} cells[10,32]. Scale bar, 20 μm. Right: bar graph for showing the percentage of eArch3.0-EYFP^{+} neurons co-expressing tdTomato ($N = 4$ mice). **b**, Ex vivo whole-cell patch-clamp recording of a representative PVN-CRF$^{eArch3.0}$ cell showing optogenetic inhibition. Left: image of a recorded cell. eArch3.0-EYFP (green), Alexa Fluor 594 (red), 60× magnification (upper: scale bar, 20 μm) and 5× magnification (lower: scale bar, 100 μm). Right: response of a PVN-CRF$^{eArch3.0}$ cell to 1 s of light pulse (green bar) under 30 pA of inward current injection in current-clamp (upper) and voltage-clamp (lower) modes. Similar responses were observed in all six other recorded cells. **c**, Schematic diagram for RTPP experiment. Closed-loop photoinhibition was delivered on conditioning days. **d**, Representative locomotor traces from a PVN-CRF$^{eArch3.0}$ mouse receiving photoinhibition at 532 nm (green bars) before and after conditioning (upper) and after each day of conditioning (bottom). **e**, Normalized place preference index (%) for the photoinhibition-paired side: average preference indices (%) from PVN-CRF$^{eArch3.0}$ mice (green) and control PVN-CRF^{eYFP} mice (gray). Inset: average preference indices for mice that received photoinhibition on the first day of conditioning in 5 min time bins. Whisker box plot from minimum to maximum. **f**, Raw individual place preference indices (%) of PVN-CRF^{eArch3} ($N = 11$, green) and PVN-CRF^{eYFP} ($N = 8$, gray) mice before and after conditioning. The photoinhibition-paired chamber is chosen based on the mouse's initial aversion to the chamber. $^{*}P < 0.05$, $^{**}P < 0.01$, $^{***}P < 0.001$, $^{****}P < 0.0001$. Data are presented as mean ± s.e.m.

mice started to demonstrate a preference for the photoinhibition-paired chamber within the first 5 minutes of conditioning and the preference became statistically significant after 15 minutes (Fig. 5e). On the subsequent days of conditioning and testing day, the mice continuously showed a preference for the chamber in which PVN CRF neurons were inhibited (Fig. 5e,f). This result suggests that mice can quickly learn the effect of inhibited PVN CRF neuronal activity or, alternatively, may be exhibiting an innate appetitive response that was prompted by the rapid drop of PVN CRF neuronal activity. Because the RTPP behavioral paradigm allows mice to freely and rapidly explore two chambers, the release of CRF peptide or the level of peripheral stress hormone, CORT, that is noticeable in minutes[17] is unlikely to encode positive or negative valence.

Optogenetic activation or inhibition of PVN CRF neuronal activity blunts a preference to food or an aversion to LiCl injection. We further examined whether the activity of PVN CRF neurons is important for mediating behavioral responses to naturally occurring stimuli. We first tested whether simultaneous activation of PVN CRF neurons during exposure to food, which reduces their neuronal activity (Fig. 2), can override animals' preference to the food-paired context. To this end, we optogenetically activated PVN CRF neurons of a food-restricted mouse (PVN-CRF$^{ChR2\ or\ eYFP}$) whenever the mouse entered one of the preassigned two chambers that contained a chow pellet. Each conditioning session lasted for 30 minutes once a day for 4 days and mouse's preference for either chamber was probed in the absence of food or optical stimulation on the testing day (Fig. 6a). In comparison to the control PVN-CRF^{eYFP} mice, which developed a strong preference for the food-paired chamber (Fig. 6b–d), PVN-CRF^{ChR2} mice showed a significant reduction in preference on the first day of conditioning and subsequent days (Fig. 6b–d). Even when PVN-CRF^{ChR2} mice chose to stay in the food-paired chamber, the mice spent less time in eating (Fig. 6e and Supplementary Fig. 10a,d), probably because they did not initiate feeding bouts as frequently as the control mice (Fig. 6f,g and Supplementary Fig. 10b,e). However, activation of PVN CRF neurons did not reduce the duration of each feeding epoch once a feeding bout was started (Fig. 6h and Supplementary Fig. 10c). This finding is consistent with the putative role of PVN CRF neurons in evaluating the reward value of appetitive stimuli rather than mediating the consummatory action of food intake.

We next sought to determine whether simultaneous inhibition of PVN CRF neurons during exposure to intraperitoneal injections of LiCl, which induces visceral discomfort and increases CRF neuronal activity (Fig. 1k–m), can override mice's conditioned aversion to the LiCl-paired chamber in the CPA assay[21,22]. We conditioned each mouse (PVN-CRF$^{eArch3\ or\ eYFP}$) by injecting LiCl intraperitoneally and leaving it in a preassigned chamber for 40 minutes, followed by injecting the same mouse with saline and leaving it in the other chamber for 40 minutes 6 hours later (Fig. 7a). During the period in which PVN-CRF^{eArch3} mice were in the LiCl-paired chamber, they received green light stimulation, which inhibits the

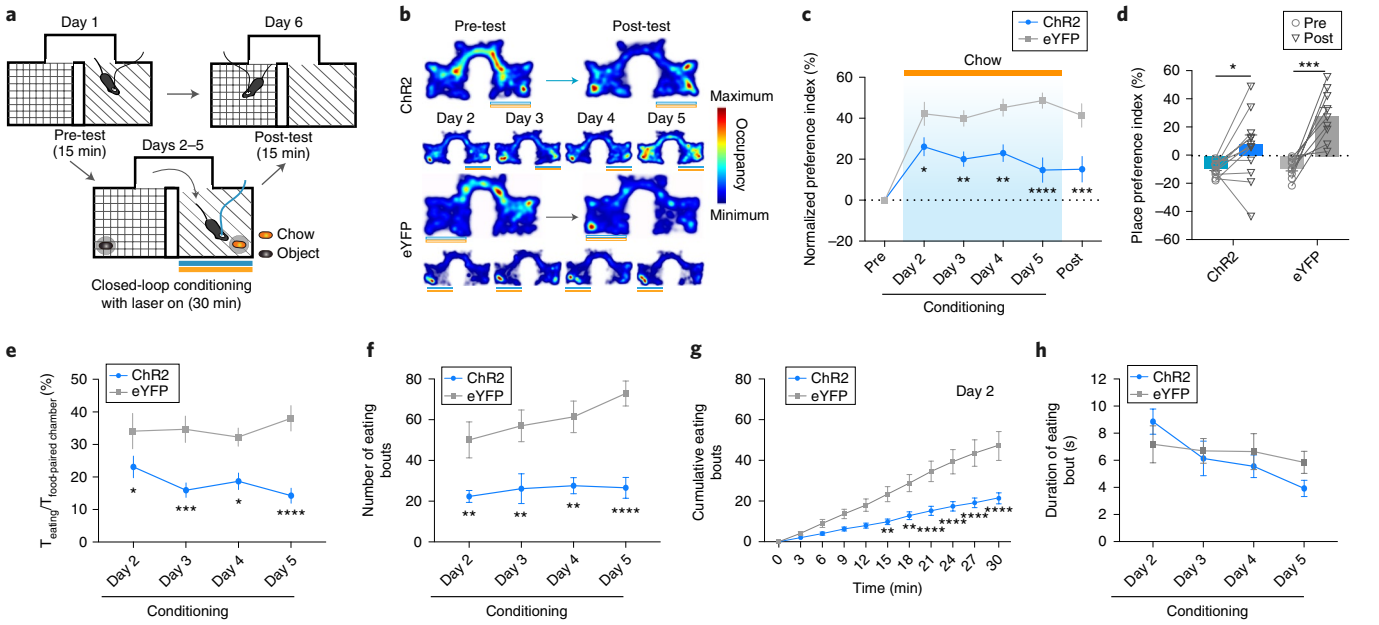

Fig. 6 | Simultaneous activation of PVN CRF neurons reduces food preference and food-induced CPP. a, Schematic of food-induced RTPP experiment with optogenetic activation. Closed-loop light stimulation at 473 nm was delivered in the food-paired chamber, but not in the object-paired chamber, on conditioning days. **b**, Representative locomotor traces from PVN-CRF^{ChR2} (upper) and PVN-CRF^{eYFP} (lower) mice that were given food with simultaneous photostimulation before and after conditioning (upper) and after each day of conditioning (bottom). **c**, Normalized place preference index (%) for the food-photostimulation-paired side: average preference indices of PVN-CRF^{ChR2} (blue) and control PVN-CRF^{eYFP} (gray) mice. **d**, Raw place preference indices (%) of PVN-CRF^{ChR2} mice ($N=12$, blue) and PVN-CRF^{eYFP} mice ($N=9$, gray) before and after conditioning. **e**–**h**, Time spent in eating normalized to time spent in the food-paired chamber (%) (**e**), the number of eating bouts (**f**), the cumulative bouts on day 2 (**g**), and the duration of each eating bout (**h**) of PVN-CRF^{ChR2} mice ($N=12$, blue) and control PVN-CRF^{eYFP} ($N=9$, gray) mice. $^{*}P<0.05$, $^{**}P<0.01$, $^{***}P<0.001$, $^{****}P<0.0001$. Data are presented as mean ± s.e.m.

activity of PVN CRF neurons. Each mouse was conditioned for 3 days before probing its preference on the testing day. In control PVN-CRF ^{eYFP} mice, LiCl injections induced significant CPA as shown by a decrease in the time spent in the LiCl-paired chamber (Fig. 7b–d) and an increased probability of U-turning when they moved from the saline-paired chamber towards the entrance of the LiCl-paired chamber (Fig. 7e,f). In contrast, inhibition of PVN CRF neuronal activity during the conditioning days eliminated the CPA (Fig. 7b–d) and higher probability of U-turn at the entrance of the LiCl-paired chamber (Fig. 7e,f) in PVN-CRF^{eArch3} mice. Together, these functional studies revealed that an increase or a decrease in the activity of PVN CRF neurons is essential for guiding aversive or approach responses to natural stimuli, probably through a fast-acting HPA-independent pathway.

Discussion

Our fiber photometry recordings of PVN CRF neurons in freely behaving mice suggest that these neurons mediate rapid detection of a wide range of aversive and appetitive stimuli. PVN CRF neurons are immediately activated by aversive cues and inhibited by appetitive stimuli. Furthermore, optogenetic manipulations of PVN CRF neuronal activity were sufficient to induce conditioned aversion or preference towards initially neutral contexts. Intriguingly, simultaneous activation or inhibition of PVN CRF neurons during exposure to appetitive or aversive stimuli can override animals' behavioral responses to these stimuli.

The role of PVN CRF neurons in mediating rapid sensory detection and regulating the neuroendocrine axis closely resembles the feedforward property of hypothalamic neurons. For instance, AgRP hypothalamic neurons regulate energy homeostasis but also respond quickly to food-derived sensory cues such as food odor[23–25]; SFO^{Nos1} neurons regulate fluid homeostasis, but also respond rapidly to water ingestion even before the water reaches circulation[26]. Each of these may represent a straightforward means of quickly pairing the physiological needs of the body with the anticipation of finding food or water in the environment. The speed with which both aversive and attractive stimuli are detected by PVN CRF neurons may serve as an effective way to immediately activate approach or avoidance behavior, and also reset their ongoing regulation of the neuroendocrine HPA axis. That PVN CRF neurons harbor the feedforward property with a more general theme of aversion and approach would expand the scope of the pathway and enhance survival and reproductive advantages in animals.

In fact, the speed with which mice display defensive behaviors following stress is at odds with the slow neuroendocrine response to stress. Thus, it is likely that the immediate activation of PVN CRF neurons is necessary to trigger rapid defensive behavior. Indeed, acute photostimulation of PVN CRF neurons in mice was followed by behavioral responses similar to those that are typically observed at the onset of acute stress, such as grooming[17,27]. Our finding that optogenetic stimulation of PVN CRF neurons promotes CPA or learned aversion is consistent with previous findings that activation of this pathway results in aversive responses[6,7,17]. Furthermore, the observation that CRF knockout mice still exhibited grooming behavior following stress suggests that this stress-induced behavior is mediated by a pathway that is independent of the HPA axis[28]. This view is consistent with our finding that rapid conditioning of mice in an RTPA arena tracks well with quick stimulation of PVN CRF neuronal activity, and thus is less likely due to slow rise of molecular CRF or glucocorticoid levels.

Our in vivo recordings unexpectedly revealed that the activity of PVN CRF neurons is rapidly and potently suppressed by appetitive stimuli such as food and pups. Previously, quantitative immune-electron microscopy studies illustrated that approximately half of

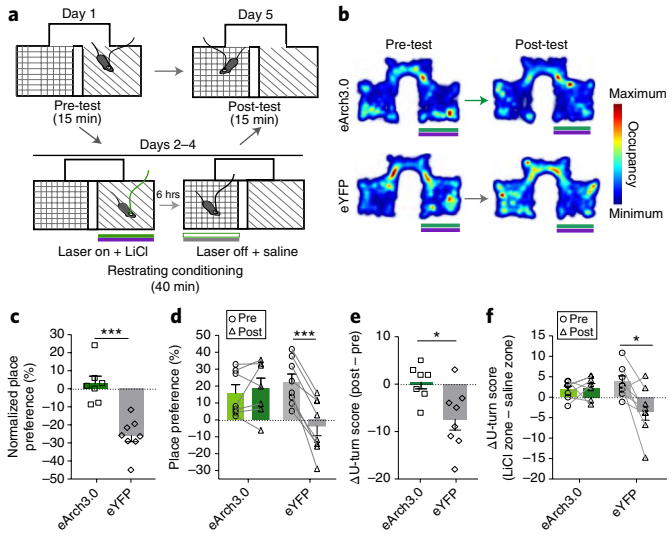

Fig. 7 | Simultaneous inhibition of PVN CRF neurons abolishes the LiCl-induced CPA. a, Schematic diagram for LiCl-induced CPA with optogenetic inhibition at 532 nm. Mice that received an injection of LiCl and concurrently received photoinhibition in one chamber; mice that received an injection of saline in the other side did not receive photoinhibition on conditioning days. **b**, Representative locomotor traces from PVN-CRF$^{eArch3.0}$ (upper) and PVN-CRF^{eYFP} (lower) mice that received LiCl injections with simultaneous photoinhibition before and after conditioning. **c**, Normalized place preference (%) for the LiCl/photoinhibition-paired side: average preference indices of PVN-CRF$^{eArch3.0}$ mice (green) and control PVN-CRF^{eYFP} mice (gray). **d**, Raw place preference indices (%) of PVN-CRF$^{eArch3.0}$ ($N=7$, green) and PVN-CRF^{eYFP} ($N=8$, gray) mice for the LiCl-paired chamber before and after conditioning. The LiCl-paired chamber is chosen based on the mouse's initial preference to the chamber. **e**,**f**, The differences between ΔU-turn scores before conditioning and ΔU-turn scores after conditioning (**e**), and the differences between raw U-turn scores at the entrance of the LiCl-paired chamber and raw U-turn scores at the entrance of the saline-paired chamber, before and after conditioning (**f**) of PVN CRF$^{eArch3.0}$ (green, $N=7$) and PVN CRF^{eYFP} (gray, $N=8$) mice. $^{*}P<0.05$, $^{***}P<0.001$. Data are presented as mean ± s.e.m.

all synapses onto PVN CRF neurons are GABAergic; the other half being glutamatergic[29]. While the glutamatergic input potentiates PVN CRF neuronal activity, the GABAergic inputs were proposed to modulate glutamate-induced activation of the HPA axis[30,31]. Our findings that PVN CRF neuronal inhibition by appetitive stimuli occurs as rapidly as CRF neuronal activation by aversive cues and that artificial silencing of PVN CRF neurons promotes a CPP within several minutes of conditioning argue for substantive GABAergic inputs that allow efficient encoding of appetitive signals. Identification of functionally relevant glutamatergic and GABAergic inputs onto PVN CRF neurons will be an important topic to pursue in the future.

The biphasic characteristics of PVN CRF neurons resemble those of dopaminergic neurons in the ventral tegmental area (VTA) that are activated and inhibited by rewarding and aversive stimuli, respectively[3]. Activation of VTA dopaminergic neurons that stimulate the dopamine D1 receptor-expressing neurons in the nucleus accumbens, the direct pathway, is essential for encoding reward signals[4]. By contrast, inhibition of VTA dopaminergic neurons results in mediating aversive responses that require the dopamine D2 receptor, which is the key mediator in the indirect pathway[5]. This valence coding strategy is distinct from those involving topographically segregated populations of neurons that mediate positive and negative reinforcement independently[1,2]. Further studies will need to clarify the molecular and circuit mechanisms by which PVN CRF neurons mediate rapid behavioral responses to aversive and attractive cues, and may lead to a comprehensive understanding of how animals respond to competing environmental stimuli.

Online content

Any methods, additional references, Nature Research reporting summaries, source data, statements of data availability and associated accession codes are available at https://doi.org/10.1038/s41593-019-0342-2.

Received: 10 April 2018; Accepted: 18 January 2019;
Published online: 04 March 2019

References

1. Namburi, P., Al-Hasani, R., Calhoon, G. G., Bruchas, M. R. & Tye, K. M. Architectural representation of valence in the limbic system. *Neuropsychopharmacology* **41**, 1697–1715 (2016).
2. Tye, K. M. Neural circuit motifs in valence processing. *Neuron* **100**, 436–452 (2018).
3. Ungless, M. A., Magill, P. J. & Bolam, J. P. Uniform inhibition of dopamine neurons in the ventral tegmental area by aversive stimuli. *Science* **303**, 2040–2042 (2004).
4. Tsai, H. C. et al. Phasic firing in dopaminergic neurons is sufficient for behavioral conditioning. *Science* **324**, 1080–1084 (2009).
5. Danjo, T., Yoshimi, K., Funabiki, K., Yawata, S. & Nakanishi, S. Aversive behavior induced by optogenetic inactivation of ventral tegmental area dopamine neurons is mediated by dopamine D2 receptors in the nucleus accumbens. *Proc. Natl Acad. Sci. USA* **111**, 6455–6460 (2014).
6. Bains, J. S., Wamsteeker Cusulin, J. I. & Inoue, W. Stress-related synaptic plasticity in the hypothalamus. *Nat. Rev. Neurosci.* **16**, 377–388 (2015).
7. Ulrich-Lai, Y. M. & Herman, J. P. Neural regulation of endocrine and autonomic stress responses. *Nat. Rev. Neurosci.* **10**, 397–409 (2009).
8. Gunaydin, L. A. et al. Natural neural projection dynamics underlying social behavior. *Cell* **157**, 1535–1551 (2014).
9. Cui, G. et al. Concurrent activation of striatal direct and indirect pathways during action initiation. *Nature* **494**, 238–242 (2013).
10. Wamsteeker Cusulin, J. I., Füzesi, T., Watts, A. G. & Bains, J. S. Characterization of corticotropin-releasing hormone neurons in the paraventricular nucleus of the hypothalamus of Crh-IRES-Cre mutant mice. *PLoS One* **8**, e64943 (2013).
11. Yilmaz, M. & Meister, M. Rapid innate defensive responses of mice to looming visual stimuli. *Curr. Biol.* **23**, 2011–2015 (2013).
12. Fendt, M., Endres, T., Lowry, C. A., Apfelbach, R. & McGregor, I. S. TMT-induced autonomic and behavioral changes and the neural basis of its processing. *Neurosci. Biobehav. Rev.* **29**, 1145–1156 (2005).
13. Golden, S. A., Covington, H. E. III, Berton, O. & Russo, S. J. A standardized protocol for repeated social defeat stress in mice. *Nat. Protoc.* **6**, 1183–1191 (2011).
14. Seip, K. M. & Morrell, J. I. Exposure to pups influences the strength of maternal motivation in virgin female rats. *Physiol. Behav.* **95**, 599–608 (2008).
15. Boyden, E. S., Zhang, F., Bamberg, E., Nagel, G. & Deisseroth, K. Millisecond-timescale, genetically targeted optical control of neural activity. *Nat. Neurosci.* **8**, 1263–1268 (2005).
16. Aravanis, A. M. et al. An optical neural interface: in vivo control of rodent motor cortex with integrated fiberoptic and optogenetic technology. *J. Neural. Eng.* **4**, S143–S156 (2007).
17. Füzesi, T., Daviu, N., Wamsteeker Cusulin, J. I., Bonin, R. P. & Bains, J. S. Hypothalamic CRH neurons orchestrate complex behaviours after stress. *Nat. Commun.* **7**, 11937 (2016).
18. Tan, K. R. et al. GABA neurons of the VTA drive conditioned place aversion. *Neuron* **73**, 1173–1183 (2012).
19. Chow, B. Y. et al. High-performance genetically targetable optical neural silencing by light-driven proton pumps. *Nature* **463**, 98–102 (2010).
20. Mattis, J. et al. Principles for applying optogenetic tools derived from direct comparative analysis of microbial opsins. *Nat. Methods* **9**, 159–172 (2011).
21. Yasoshima, Y., Scott, T. R. & Yamamoto, T. Differential activation of anterior and midline thalamic nuclei following retrieval of aversively motivated learning tasks. *Neuroscience* **146**, 922–930 (2007).
22. Zhu, Y., Wienecke, C. F. R., Nachtrab, G. & Chen, X. A thalamic input to the nucleus accumbens mediates opiate dependence. *Nature* **530**, 219–222 (2016).
23. Betley, J. N. et al. Neurons for hunger and thirst transmit a negative-valence teaching signal. *Nature* **521**, 180–185 (2015).
24. Chen, Y., Lin, Y. C., Kuo, T. W. & Knight, Z. A. Sensory detection of food rapidly modulates arcuate feeding circuits. *Cell* **160**, 829–841 (2015).

25. Mandelblat-Cerf, Y. et al. Arcuate hypothalamic AgRP and putative POMC neurons show opposite changes in spiking across multiple timescales. *eLife* **4**, 4 (2015).
26. Zimmerman, C. A. et al. Thirst neurons anticipate the homeostatic consequences of eating and drinking. *Nature* **537**, 680–684 (2016).
27. Spruijt, B. M., van Hooff, J. A. & Gispen, W. H. Ethology and neurobiology of grooming behavior. *Physiol. Rev.* **72**, 825–852 (1992).
28. Dunn, A. J. & Swiergiel, A. H. Behavioral responses to stress are intact in CRF-deficient mice. *Brain Res.* **845**, 14–20 (1999).
29. Miklós, I. H. & Kovács, K. J. GABAergic innervation of corticotropin-releasing hormone (CRH)-secreting parvocellular neurons and its plasticity as demonstrated by quantitative immunoelectron microscopy. *Neuroscience* **113**, 581–592 (2002).
30. Cole, R. L. & Sawchenko, P. E. Neurotransmitter regulation of cellular activation and neuropeptide gene expression in the paraventricular nucleus of the hypothalamus. *J. Neurosci.* **22**, 959–969 (2002).
31. Hewitt, S. A., Wamsteeker, J. I., Kurz, E. U. & Bains, J. S. Altered chloride homeostasis removes synaptic inhibitory constraint of the stress axis. *Nat. Neurosci.* **12**, 438–443 (2009).
32. Walker, L. C., Cornish, L. C., Lawrence, A. J. & Campbell, E. J. The effect of acute or repeated stress on the corticotropin releasing factor system in the CRH-IRES-Cre mouse: a validation study. *Neuropharmacology* https://doi.org/10.1016/j.neuropharm.2018.09.037 (2018).

Acknowledgements

We are grateful to K. Narasimhan, L. Vendruscolo, and members of the Suh laboratory for critical comments on the manuscript. We also thank G. Schwartz, S. Han, J. Kim, and A. Watts for discussions of this work. We appreciate W. Jung for assisting with immunohistochemistry and data analysis, and the laboratory of the late W. Vale for providing an aliquot of anti-CRF antibody. This work is supported by the TJ Park Science Fellowship of the POSCO TJ Park Foundation and the KAIST Innovative Doctoral Research Fellowship to J.K., NIH grants (R01MH101377 to D.L. and R01DK106636 to G.S.B.S.), and KAIST Chancellor's fund to G.S.B.S. and J.W.S.

Author contributions

G.S.B.S., D.L., and J.K. conceived the project, designed the experiments, and interpreted the results. G.S.B.S. wrote the manuscript with D.L., J.K. and S.L. J.K. performed the experiments with assistance from S.L., Y.-Y.F., A.S., S.P., S.B., and D.K. J.K. and D.L. analyzed the calcium imaging data. Y.-Y.F., K.H., and D.L. made it possible for J.K. to carry out fiber photometry recordings.

Competing interests

The authors declare no competing interests.

Additional information

Supplementary information is available for this paper at https://doi.org/10.1038/s41593-019-0342-2.

Reprints and permissions information is available at www.nature.com/reprints.

Correspondence and requests for materials should be addressed to D.L. or G.S.B.S.

Journal peer review information: *Nature Neuroscience* thanks Stephen Mahler and other anonymous reviewer(s) for their contribution to the peer review of this work.

Publisher's note: Springer Nature remains neutral with regard to jurisdictional claims in published maps and institutional affiliations.

Methods

Mice. All animal experiments were performed according to protocols approved by Institutional Animal Care and Use Committees protocols from New York School of Medicine and Korea Advanced Institute of Science and Technology for the care and use of laboratory animals. We complied with all pertinent ethical regulations. We used CRF-ires-Cre mice (B6(Cg)-*Crh*$^{tm1(cre)Zjh}$/J; Jackson Laboratory, stock no. 012704) and CRF:Ai14, crossed from homozygous CRF-ires-cre and Ai14 (B6(Cg)-*Gt(ROSA)26Sor*$^{tm14(CAG-tdTomato)Hze}$/J; Jackson Laboratory, stock no. 007914), both female and male (8–16 weeks old), housed individually under a 12-h light/dark cycle (7:00 to 19:00 light), with food and water available ad libitum unless specified. CD-1 mice (Charles River Laboratory), aged over 3 months, were used for behavior testing with an aggressive intruder.

Stereotaxic surgery. AAV1-CAG-Flex-GCaMP6s virus (120 nl, 1.9×10^{13} genomic copies per ml, University of Pennsylvania Vector Core) was stereotaxically injected unilaterally into the PVN (bregma ML: 0.2 mm, AP: −0.75 mm, DV: −4.7 mm from the brain skull) of CRF-ires-Cre mice using a Nanoject III (Drummond). In the same surgery, a mono fiber-optic cannula (5 mm, core diameter = 400 µm, numerical aperture of 0.48; Doric lenses, MFC_400/430-0.48_5mm_ZF2.5_FLT) was implanted above the PVN (−4.3 mm DV) and sealed with dental cement (C&B Metabond, S380). Stereotaxic surgery for optogenetic manipulations is described in the section 'In vivo optogenetic activation or inhibition'. Animals received intraperitoneal injection of 5 mg kg^{-1} ketoprofen after the surgery and were singly housed to recover for 3–4 weeks before testing.

Fiber photometry recording. The fiber photometry setup was constructed as previously described[8,33]. Briefly, a 400-Hz sinusoidal 473 nm blue light-emitting diode (30 µW) (light-emitting diode: M470F1; light-emitting diode driver: LEDD1B, Thorlabs) was bandpass filtered (passing band: 472 ± 15 nm, Semrock, FF02-472/30–25) and used to excite GCaMP6s fluorescence. A dichroic mirror was used to reflect 473 nm and pass the emission light from the activated GCaMP6s fluorescence. Bandpass-filtered light (passing band: 535 ± 25 nm, Semrock, FF01–535/50–25) was detected by a femto-watt silicon photodetector (Newport, 2151) and recorded as digitized signal using a real-time processor (RP2.1, TDT). The real-time signal was time-locked following the same time frame from the video recording system using StreamPix, such that the acquired signals and the monitored episodic behaviors of the animals could be synchronized.

The normalized GCaMP fluorescence signals (F_n) were calculated from dividing the raw GCaMP signals by the mean fluorescence signals from −100 s to ~−5 s before the stimulus presentation.

For the peri-event time histograms (PETHs), the onsets of each event were aligned to the time zero and the signals were normalized as $(F-F_{baseline})/F_{baseline}\times100$ ($\Delta F/F$ (%)). $F_{baseline}$ was the mean of GCaMP signals for the window before the time zero. F is the mean of GCaMP6 signals for the window after the time zero.

For the population plots, $F_{baseline}$ was calculated from −100 s to ~−5 s before the introduction of stimulus to exclude the increased signals due to the placement of stimuli in the box.

Average $\Delta F/F$ (%) values in bar graphs were calculated as $(F_{duration}-F_{baseline})/F_{baseline}\times100$. For Fig. 1j (TRT and overhead) and Fig. 3g, where stimuli were given short-term, $F_{baseline}$ is the mean of GCaMP signal for 5 s before time zero and $F_{duration}$ is the mean of GCaMP signal for the duration of the annotated period.

In Fig. 1j (FST and TMT) and Figs. 2b,e,h and 3b, where stimuli were presented long-term, $F_{baseline}$ is the mean of GCaMP signal for 300 s (or 100 s for TMT) before time zero and $F_{duration}$ is the mean of GCaMP signal for the entire session of given stimuli—object, chow, object/cup, chow/cup (where chow is present but inaccessible), peanut butter/cup (where peanut butter is present but inaccessible), peanut butter, and pup.

In Fig. 2k,l, the decay time constant during the initial phase of drop in GCaMP signal was obtained as the duration between the onset of stimulus presentation and the time at which the GCaMP6 signal reached 63.2% of the maximal change.

In Supplementary Figs. 4b and 6, the frequency of calcium transients was calculated as the number of peaks over threshold, 30% of (maximum − minimum), for 10 min of each duration.

Video recording and behavioral analysis. All behavioral experiments were performed in a custom-made behavior chamber with air-fan and under dimmed light (for visual cue or CPP experiment) or infrared illumination from the start of dark cycle. Mice were habituated in the chamber for 20 min before each experiment. Their behaviors were video-taped using two synchronized infrared cameras (Basler, ace120gc) placed from the top/side of the chamber and a commercial acquisition software (StreamPix 6, Norpix) at a frame rate of 25 frames per second. Manual behavior annotation was executed on a frame-by-frame basis with Caltech behavior annotator code written in MATLAB[34]. Detailed behavioral annotations are described in Supplementary Table 2. The behavior annotation was time-locked with the recorded GCaMP6 signal and plotted as a bar plot under its trace using MATLAB.

FST. We used the protocol for FST that was described previously[35,36]. Briefly, the animal was gently placed into a 3-l beaker (18 cm in height) filled with 24–25 °C water until 12 cm deep. After 6 min forced swimming, the mice were gently dried by paper towel and placed back in their home cage.

TRT. The tail of tested mice was chased and grabbed by hand. After grabbing, the mice were suspended in air for 6–8 s before releasing them in their home cage.

Presentation of a looming cue. A large bird-like object was custom made and presented as a cue that moves above or lateral to the cage. For more systematic presentations of a visual cue, we engineered a looming shadow disk as previously reported[11]. The looming shadow disk panel was placed at the bottom, side, or top of a transparent cage ($25\times25\times30$ cm^3) sequentially with 10 min of interval after 15 min of habituation. The looming disk was programmed as a black circle in a gray background, increasing its size from 2 degrees of visual angle expanding to 20 degrees in 250 ms, maintained for 250 ms, and presented repeatedly 15 times with 500 ms of interval for 1 trial.

Presentation of odorants. Mice were habituated for 10 min in a chamber box ($20\times20\times20$ cm^3) equipped with an air-fan. A piece of 2-cm^2 filter paper soaked with 40 µl of either water or 1:10 diluted 2,5-dihydro-2,4,5-trimethylthiazoline (Sigma Aldrich) was presented gently at the center of the chamber as described[37]. The odorants were presented for 5 min with 15 min of interval.

Intraperitoneal administration of LiCl. After 20 min of habituation for the optic fiber in its home cage, a tested mouse was briefly put into an anesthesia chamber with isoflurane and then given intraperitoneal injection of LiCl (125 mg kg^{-1}), followed by placing back into its home cage. Saline (0.9%, in the same volume, 10 µl per gram of body weight) was given as control.

Presentation of food or food cues. On day 1, baseline activity in ad libitum fed state was measured for 1 h in a chamber ($20\times20\times20$ cm^3, equipped with water sipper). Following 1 h of recording in the chamber, the tested animal was deprived of food with ad libitum water for 22 h in their home cage. On day 2, the fasted animal was replaced into the behavior chamber and habituated for 15 min. After the habituation, a small object (~1 cm^3) was presented for 15 min as a control and then a small pellet of food (4 g per pellet) was placed.

For the inaccessible food condition, mice were habituated in the chamber equipped with a mesh-covered cup (9 cm diameter, 3 cm height). The object or chow pellet was placed under the mesh-covered cup for 10 min, followed by free access to the chow pellet. Peanut butter (Kirkland, purchased from Costco) was used alone or with the mesh-covered cup.

For comparing the baseline of PVN-CRF^{GCaMP6} signals, mice in ad libitum fed sate were recorded for about 20 min after habituation to the optic fiber, followed by fasting for 22 h and the sequential measurement of the baseline then given with chow pellet. Average signals from the last 10 min were calculated.

For c-Fos labeling, the brains of mice that were starved for 9 h and 22 h (and were killed at the same time) were co-immunostained with anti-c-Fos and anti-CRF antibodies (from the laboratory of late Wylie Vale).

Resident–intruder social interaction. To observe social interactions and PVN CRF neuronal activity in vivo, different intruders were brought into the home cage of recorded mice. A pup (< 2 weeks) was carefully presented to a recorded mouse (male or virgin female) to observe interaction with pups. An aggressive CD1 male or lactating female intruder was selected as previously reported, with attack within 3 min after introduction[13]. The same CD1 aggressor was introduced into the home cage of the recorded males on different days. As a control, fake animal, a mouse-like object similar in size to an adult B6 mouse was used.

In vivo optogenetic activation or inhibition. For optimal conditions for optogenetic modulation of PVN CRF neuronal activity, we referred to ref. [17]. To express ChR2 in PVN CRF neurons, 120 nl AAV2-EF1a-DIO-ChR2-EYFP (4.0×10^{13} genomic copies per ml, University of North Carolina Vector Core) was unilaterally injected into the PVN (Bregma ML: 0.2 mm, AP: −0.75 mm, DV: −4.7 mm from the brain skull) of CRF-ires-cre:Ai14 mice (2–3 months). To express eArch3.0 in PVN CRF neurons, 120 nl AAV2-EF1a-DIO-eArch3.0-EYFP (University of North Carolina Vector Core) was bilaterally injected into the PVN. The control mice were injected with AAV5-EF1a-DIO-eYFP (2.7×10^{12} genomic copies per ml, University of North Carolina Vector Core). During the surgery, mono fiber-optic cannulas (200 µm diameter, numerical aperture of 0.48, Doric Lenses) were implanted 300–400 µm above the target area (ML: 0.2 mm, AP: −0.75 mm, DV: −4.3 mm from the skull for PVN-CRF$^{ChR2\ or\ eYFP(uni)}$ group; ML: 0.0 mm, AP: −0.75 mm, DV: −4.3 mm for PVN-CRF$^{eArch3.0\ or\ eYFP(bi)}$ group) and were secured with dental cement (C&B Metabond, S380). Light from a 473-nm diode-pumped solid-state laser (CrystaLaser) was delivered through a fiber-optic patch cord (Doric Lenses) at 10 Hz, 10 ms of pulse width, 15 mW of light intensity at the tip of the optic fiber. Light from a 532-nm diode-pumped solid-state laser (CrystaLaser) was continuously delivered with 15 mW of light intensity. Light pulses were controlled by a pulse generator (Agilent).

For c-Fos labeling of activated CRF neurons on photostimulation, the mice injected with AAV-EF1a-DIO-ChR2 were given the blue light (473 nm, 10 ms,

10 Hz) for 5 min in their home cage and killed 90 min after the light turned off. Brains from these mice were immunostained for c-Fos antibody as in the following protocols.

Closed-loop CPA/CPP. The custom-made CPA/CPP apparatus consisted of two rectangular chambers ($20 \times 18\ cm^2$) with distinct wall drawings, and a corridor separating them was used. Tracks of mouse movement were recorded with a charge-coupled device (CCD) camera and analyzed with EthoVision XT 8.5/14 software (Noldus) using its center-point feature. For the protocol of CPA/CPP tests, we referred to ref. [18]. Briefly, on day 1, before conditioning, mice freely explored the chambers for 15 min without light. We excluded mice showing place bias higher than 25% (except one eArch3.0 mouse). Over the following 4 days of conditioning, mice were trained for 30 min with light given in 1 chamber. The light-paired chamber was determined by the side with higher preference on day 1 for photostimulation, whereas the side with lower preference on day 1 for photoinhibition. The light was triggered whenever mice entered the light-paired chamber by transitor-transitor logic (TTL) signal using the mini I/O box with EthoVision XT package (Noldus). To avoid overheating of the brain tissue in use with 473-nm laser, photostimulation ceased if mice stayed in the light-paired chamber longer than 30 s. If mice continued to stay in the light-paired chamber 1 min after the light pulse turned off, photostimulation was turned on again. On day 6, as post-test, mice were allowed to explore the chambers for 15 min without light.

Place preference index (%) was calculated as (Time spent in the light-paired chamber − Time spent in the light-unpaired chamber)/(Time spent in either chamber) × 100. Normalized place preference (%) was calculated as difference between place preference index on each day and the pretest day to illustrate the development of avoidance/preference compared with the pretest day.

$$\text{Place preference index (\%)} = \frac{(T_{\text{light-paired chamber}} - T_{\text{light-unpaired chamber}})}{(T_{\text{light-paired chamber}} + T_{\text{light-unpaired chamber}})} \times 100$$

$$\text{Normalized place preference}_{\text{Day}}(\%) = \text{Place preference index}_{\text{Day}} - \text{Place preference index}_{\text{Pre-test}}$$

Food-induced CPP while activating PVN CRF neurons. Food-induced CPP was conducted in the same custom-made CPA/CPP apparatus used for the closed-loop CPA/CPP test described above. Food was provided in a cage and mice were restricted to approximately 80% of their daily food intake for 6 d from 1 d before conditioning until the post-test. On day 1, before conditioning, mice were allowed to freely explore the entire chamber for 15 min without photostimulation or food. Over the following 4 d of conditioning, mice were trained for 30 min in two distinct chambers; one paired with food in a cage and blue photostimulation (473 nm) and the other with an object in a cage and no photostimulation. The side for which the mice showed lower preference on day 1 was set as the side to contain food and blue photostimulation. The food was placed in a cage such that the mice could consume it but not translocate it. Whenever mice entered the chamber paired with food, blue photostimulation (473 nm, 10 Hz, 10 ms) was delivered for 1 min intervals, with 30 s breaks in between. One hour after the end of each training session, mice were given restricted amounts of food to avoid mnemonic effects of food[38,39]. On day 6, after conditioning, mice were allowed to explore the chambers for 15 min without photostimulation or food.

For the time-resolved analysis, feeding bouts were manually annotated on a frame-by-frame basis using Caltech behavior annotator, and the time frame was matched with time and position of the subject from EthoVision to calculate average duration of eating bout(s), time spent in eating normalized to time spent within the food-paired chamber (%), and the probability of initiating eating when the subject presented in the food-paired chamber (%).

LiCl-induced CPA while inhibiting PVN CRF neurons. For LiCl-induced CPA, we modified the protocol used in refs. [21,22]. On day 1, before conditioning, mice (PVN-CRF$^{eArch3.0}$ or PVN-CRF^{eYFP}) were allowed to freely explore the custom-made CPP apparatus and their basal place preference was observed. Over the following 3 d of conditioning, mice were given intraperitoneal injections of saline under brief anesthesia with isoflurane and confined to 1 side of the chamber for 40 min and then put back into their home cage. Six hours later, the same mice received green photoinhibition (532 nm) and an intraperitoneal injection of LiCl ($125\ mg\ kg^{-1}$) then were confined to the other side of the chamber for 40 min. These 2 sessions were performed once per day for 3 d and the order (saline-LiCl) was counterbalanced and randomized between individuals. On day 5, mice were re-exposed to freely move between both sides of the CPP apparatus for 15 min.

U-turn score was counted as the number of zone transitions (for example, zone^{LiCl} to zone^{neutral} to zone^{LiCl}) of the detected subject in the EthoVision program. ΔU-turn score is the difference of the U-turn score at the entrance of zone^{LiCl} from zone^{Saline}. ΔU-turn score (Post – Pre) is the subtraction of ΔU-turn scores between before and after the conditioning days.

Slice whole-cell patch clamp recordings. AAV2-E1Fa-DIO-ChR2-EYFP (120 nl) was stereotaxically injected into PVN of CRF-ires-Cre:Ai14 mice (6 weeks).

After 3 weeks of viral incubation, mice were anaesthetized with isoflurane and transcardially perfused with a cutting solution, ice-cold modified ACSF (220 mM sucrose, 26 mM $NaHCO_3$, 2.5 mM KCl, 1 mM NaH_2PO_4, 5 mM $MgCl_2$, 1 mM $CaCl_2$, 10 mM glucose, pH 7.3–7.35). The mice were then decapitated, and the entire brain was removed and immediately submerged in the ice-cold, carbogen-saturated cutting solution. Coronal sections (250 µm) were cut from the PVN with a Leica VT1200S Vibratome and then incubated in oxygenated storage solution (123 mM NaCl, 26 mM $NaHCO_3$, 2.8 mM KCl, 1.25 mM NaH_2PO_4, 1.2 mM $MgSO_4$, 2.5 mMg $CaCl_2$, 10 mM glucose, pH 7.3–7.35) at 34 °C for at least 1 h before the patch clamp recording. Slices were transferred to the recording chamber and allowed to equilibrate for 10 min before recording. Recordings were made in the presence of a recording solution (126 mM NaCl, 26 mM, $NaHCO_3$, 2.8 mM KCl, 1.25 mM NaH_2PO_4, 1.2 mM, $MgSO_4$, 2.5 mM $CaCl_2$, 5 mM glucose, pH 7.3–7.35). The pipette solution for current clamp mode of whole-cell patch recording was modified to include an intracellular dye (Alexa Fluor 594): 120 mM K-gluconate, 10 mM KCl, 10 mM HEPES, 5 mM EGTA, 1 mM $CaCl_2$, 1 mM $MgCl_2$, 2 mM MgATP (pH 7.29). Epifluorescence was briefly used to target fluorescent cells, at which time the light source was switched to infrared differential interference contrast imaging to obtain the whole-cell recording (Nikon Eclipse FN-S2N equipped with a fixed stage and a QImaging optiMOS complimentary metal-oxide-semiconductor (CMOS) camera). Electrophysiological signals were recorded using an Axopatch 700B amplifier (Molecular Devices), low-pass filtered at 2–5 kHz, and analyzed offline on a PC with pCLAMP 10 programs (Molecular Devices). Recording electrodes had resistance of 2–6 MΩ when filled with the K-gluconate internal solutions. Photostimulation was delivered through an Optopatcher (A-M Systems), connected to a laser source (Shanghi for 473 nm and CrystaLaser for 532 nm), through a patch cord with a numerical aperture of 0.48. Light intensity at the end of the optic fiber was measured as 2.5–8.4 mW for 473 nm and 0.2–3.5 mW for 532 nm.

Immunohistochemistry. Animals were anesthetized with isoflurane and cardially perfused with 30 ml 4% PFA followed by 30 ml 0.9% saline. Brains were postfixated for 4 h in 4% PFA at 4°C and then transferred to 20% and 30% sucrose in PBS serially. Brains were coronally sectioned at 50 µm using a Leica cryostat. The sectioned brains were washed with PBS for 10 min and blocked with 2% normal donkey serum in 0.2% PBS with triton X-100 (PBST) for 1 h at room temperature. Primary antibodies, rabbit anti-CRF (1:250, the laboratory of late Wylie Vale, Salk Institute, PBL rC68) and goat anti-c-Fos (1:200, Santa Cruz, sc 52-g), in the blocking solution (2% normal donkey serum, 0.2% PBS with Triton X-100) were incubated at 4 °C for 72 h and 24 h, respectively. The sections were washed with PBS (3 × 15 min), followed by incubation of second antibodies, donkey anti-rabbit Alexa 647 (1:500, Life Technologies, A21207) or donkey anti-goat Alexa 488/647 (1:500, Life Technologies, A11055/A21447), for 1 h at room temperature. Sections were washed with PBS (2 × 15 min), stained with DAPI (1:10,000) for 6 min, mounted on slides, and covers-lipped with DAKO mounting medium. Confocal images were captured with a Zeiss LSM 780 microscope and analyzed using ImageJ. All images were taken at ×20 magnification, unless otherwise indicated in the figure legend.

To detect viral expression or c-Fos, 20× Z-stack images of 50-µm coronal slices were taken and the number of cells was manually counted using ImageJ. Then, 10× or tile-scan of 20× images were acquired to determine the position of the optic fiber and the overall viral expression. To quantify the percentage of cells in $\frac{CRF^{+}GCaMP^{+}}{GCaMP^{+}}$, $\frac{tdT^{+}ChR2^{+}}{ChR2^{+}}$, $\frac{Fos^{+}ChR2^{+}}{ChR2^{+}}$, and $\frac{tdT^{+}eArch3.0^{+}}{eArch3.0^{+}}$, at least three representative coronal sections that were examined as a part of the PVN, referenced to a specific structure such as the third ventricle and a brain atlas (bregma –0.58 mm to –0.94 mm) along the AP axis, were used. Because the majority of CRF:tdTomato cells are localized in the PVN, bregma –0.58 to –0.94 mm[39], we targeted the middle of the PVN, bregma –0.7 to –0.8 mm, with optical fiber and used the coronal sections that bear the optical track for the representative images and cell counting.

Statistics. All statistical analyses were done in MATLAB or GraphPad Prism software. No statistical methods were used to predetermine sample sizes but our sample sizes were similar to those reported in previous publications[40,41]. We have shown individual data points in all relevant figures. Comparisons between two groups were analyzed with unpaired or paired student's *t*-test for parameters that followed a normal distribution by Shapiro–Wilk normality test, $P > 0.05$. The Mann–Whitney *U*-test (independent samples) or Wilcoxon signed rank test (dependent samples) was used for data that were not normally distributed. Comparisons of three or more groups were performed using one-way analysis of variance (ANOVA) and multiple groups under multiple testing conditions were compared using two-way ANOVA. The Holm–Sidak method was used to correct for multiple comparisons. All statistical tests were two-tailed, and all significant statistical results were indicated on the figures following the conventions: $^{*}P < 0.05$, $^{**}P < 0.01$, $^{***}P < 0.001$, $^{****}P < 0.0001$. Data are presented as mean ± s.e.m. Details of statistics are documented in Supplementary Table 1.

Subjects. Littermates were randomly assigned to control or experimental groups in behavior testing used in the study. The order of behavior tests with varied stimulus presentations was randomized in the experimental groups. The experiments were

not done blindly in the study, since the experimental conditions (control versus experimental groups) are obvious to experimenters and the analyses were carried out objectively by using a tracking system and not subjective to human bias.

Reporting Summary. Further information on research design is available in the Nature Research Reporting Summary linked to this article.

Code availability

Custom code used in this study is accessible from the corresponding author upon request.

Data availability

The data that support the findings of this study are available from the corresponding author upon request.

References

33. Falkner, A. L., Grosenick, L., Davidson, T. J., Deisseroth, K. & Lin, D. Hypothalamic control of male aggression-seeking behavior. *Nat. Neurosci.* **19**, 596–604 (2016).
34. Lin, D. et al. Functional identification of an aggression locus in the mouse hypothalamus. *Nature* **470**, 221–226 (2011).
35. García-Lecumberri, C. & Ambrosio, E. Role of corticotropin-releasing factor in forced swimming test. *Eur. J. Pharmacol.* **343**, 17–26 (1998).
36. Gao, V., Vitaterna, M. H. & Turek, F. W. Validation of video motion-detection scoring of forced swim test in mice. *J. Neurosci. Methods* **235**, 59–64 (2014).
37. Saraiva, L. R. et al. Combinatorial effects of odorants on mouse behavior. *Proc. Natl Acad. Sci. USA* **113**, E3300–E3306 (2016).
38. Rubinow, M. J., Hagerbaumer, D. A. & Juraska, J. M. The food-conditioned place preference task in adolescent, adult and aged rats of both sexes. *Behav. Brain Res.* **198**, 263–266 (2009).
39. Cusulin, J. I. W., Füzesi, T., Watts, A. G. & Bains, J. S. Characterization of corticotropin-releasing hormone neurons in the paraventricular nucleus of the hypothalamus of Crh-IRES-Cre mutant mice. *PLoS One* **8**, e64943 (2013).
40. Park, S. G. et al. Medial preoptic circuit induces hunting-like actions to target objects and prey. *Nat. Neurosci.* **21**, 364–372 (2018).
41. Fang, Y. Y., Yamaguchi, T., Song, S. C., Tritsch, N. X. & Lin, D. A hypothalamic midbrain pathway essential for driving maternal behaviors. *Neuron* **98**, 192–207.e10 (2018).

nature research

Corresponding author(s): Greg S.B. Suh & Dayu Lin

Last updated by author(s): Jan 10, 2019

Reporting Summary

Nature Research wishes to improve the reproducibility of the work that we publish. This form provides structure for consistency and transparency in reporting. For further information on Nature Research policies, see Authors & Referees and the Editorial Policy Checklist.

Statistics

For all statistical analyses, confirm that the following items are present in the figure legend, table legend, main text, or Methods section.

n/a	Confirmed	
☐	☒	The exact sample size (*n*) for each experimental group/condition, given as a discrete number and unit of measurement
☐	☒	A statement on whether measurements were taken from distinct samples or whether the same sample was measured repeatedly
☐	☒	The statistical test(s) used AND whether they are one- or two-sided *Only common tests should be described solely by name; describe more complex techniques in the Methods section.*
☒	☐	A description of all covariates tested
☐	☒	A description of any assumptions or corrections, such as tests of normality and adjustment for multiple comparisons
☐	☒	A full description of the statistical parameters including central tendency (e.g. means) or other basic estimates (e.g. regression coefficient) AND variation (e.g. standard deviation) or associated estimates of uncertainty (e.g. confidence intervals)
☐	☒	For null hypothesis testing, the test statistic (e.g. *F*, *t*, *r*) with confidence intervals, effect sizes, degrees of freedom and *P* value noted *Give P values as exact values whenever suitable.*
☒	☐	For Bayesian analysis, information on the choice of priors and Markov chain Monte Carlo settings
☒	☐	For hierarchical and complex designs, identification of the appropriate level for tests and full reporting of outcomes
☒	☐	Estimates of effect sizes (e.g. Cohen's *d*, Pearson's *r*), indicating how they were calculated

Our web collection on statistics for biologists contains articles on many of the points above.

Software and code

Policy information about availability of computer code

Data collection	We listed all softwares used in the experiments and for analysis in the Methods section. We used a custom TDT program, OpenEx (Tucker-Davis Technologies) to collect the fiberphotometry signal and StreamPix6 (Norpix) for multiple camera recording. We used EthoVisionXT 8.5/14 (Noldus) to track movement of mice and send a trigger signal to the pulse generator for optogenetics. Confocal images were captured with Zen program from LSM 780 (Zeiss). Differential interference contrast imaging to obtain the whole-cell recording (Nikon Eclipse FN-S2N equipped with a fixed stage and a QImaging optiMOS CMOS camera). Electrophysiological signals were recorded using an Axopatch 700B amplifier (Molecular Devices).
Data analysis	We listed all softwares used in the experiments and for analysis in the Methods section. We used customized code written in MATLAB 2013 to annotate behavior of animals (https://github.com/pdollar/toolbox/tree/master/videos) and further analyze the time-locked photometry signal by a customized code. We used EthoVisionXT 8.5/14 to analyze and visualize the locomotor of the mice. Confocal microscopic imaging data were analyzed by ZEN2009 Light Edition and ImageJ 1.51k with custom settings. Whole-cell patch clamp data were analyzed with pCLAMP 10 programs (Molecular Devices). All statistical analysis were performed using GraphPad Prism 7. The custom codes will be available from corresponding authors upon reasonable request.

For manuscripts utilizing custom algorithms or software that are central to the research but not yet described in published literature, software must be made available to editors/reviewers. We strongly encourage code deposition in a community repository (e.g. GitHub). See the Nature Research guidelines for submitting code & software for further information.

Data

Policy information about availability of data

All manuscripts must include a data availability statement. This statement should provide the following information, where applicable:

- Accession codes, unique identifiers, or web links for publicly available datasets
- A list of figures that have associated raw data
- A description of any restrictions on data availability

The data that support the findings of this study are available from the corresponding author upon reasonable request.

Field-specific reporting

Please select the one below that is the best fit for your research. If you are not sure, read the appropriate sections before making your selection.

☒ Life sciences ☐ Behavioural & social sciences ☐ Ecological, evolutionary & environmental sciences

For a reference copy of the document with all sections, see nature.com/documents/nr-reporting-summary-flat.pdf

Life sciences study design

All studies must disclose on these points even when the disclosure is negative.

Sample size	There is no appropriate precedent to predetermine sample size, but our sample sizes in the data are similar with previous works in this field.
Data exclusions	In behavioral experiments, eight mice with poor virus expression (<5%) or fiber implantation outside (>500um) of the PVN region as described in a mouse brain atlas (Franklin & Paxinos) were excluded. The exclusion criteria were established prior to collecting and analyzing the final sets of data.
Replication	All experiments were conducted at least with 2 cohorts of animals. All mice with sufficient viral expression (>5% of PVN neurons) and correct fiber placement (within 500 um of PVN) showed qualitatively similar responses under the same behavioral test.
Randomization	Littermates were randomly assigned as control or experimental groups in behavior testing used in the study. The order of behavior tests with varied stimulus presentations was randomized in the experimental groups.
Blinding	The experiments were not done blindly in the study, since the experimental conditions (control vs experimental groups) were obvious to experimenters and the analyses were carried out is was done objectively by using a (tracking system) and not subjective to human bias. During annotation and cell counting, the experimenter iswas blind to the GCaMP6 signal or behavioral responses.

Reporting for specific materials, systems and methods

We require information from authors about some types of materials, experimental systems and methods used in many studies. Here, indicate whether each material, system or method listed is relevant to your study. If you are not sure if a list item applies to your research, read the appropriate section before selecting a response.

Materials & experimental systems

n/a	Involved in the study
☐	☒ Antibodies
☒	☐ Eukaryotic cell lines
☒	☐ Palaeontology
☐	☒ Animals and other organisms
☒	☐ Human research participants
☒	☐ Clinical data

Methods

n/a	Involved in the study
☒	☐ ChIP-seq
☒	☐ Flow cytometry
☒	☐ MRI-based neuroimaging

Antibodies

Antibodies used	We listed all antibodies used with their catalog number in Methods section of "Immunohistochemistry". Primary antibodies : Rabbit anti-CRF (PBL rC68, Paul E.Sawchenko lab;former W. Vale lab, Salk Institute) and Goat anti-cFos (sc-52-G, Santa Cruz). Secondary antibodies: Donkey anti-rabbit Alexa 647 (A21207, Life Technologies) or Donkey anti-goat Alexa 488/647 (A11055/ A21447, Life Technologies).
Validation	Primary antibodies used in this study are listed on the JCN Antibody Database. rC68 was produced in rabbit using human/rat CRF coupled to human a-globulins as immunogen. Paul E.Sawchenko lab noted that rC68 and the characterized and extensively publihsed rC70 were produced in parallel with the same dose of the identical immunogen. Reference for validation of rC70

(PMID:18067140). Information for sc-52-g (rabbit polyclonal IgG): https://www.scbt.com/scbt/product/c-fos-antibody-4?requestFrom=search

Animals and other organisms

Policy information about studies involving animals; ARRIVE guidelines recommended for reporting animal research

Laboratory animals	We described the subjects in Methods section (Subjects). CRF-ires-Cre mice (B6(Cg)-Crhtm1(cre)Zjh/J; Jackson Laboratory, stock no: 012704), Ai14 (B6(Cg)- Gt(ROSA)26Sortm14(CAG-tdTomato)Hze/J; Jackson Laboratory, stock no: 007914) mice both female and male (8-16weeks old) housed individually under a 12-hr light/dark cycle (7 am to 7 pm light), with food and water available ad libitum unless specified. CD-1 mice (Charles River Laboratory), aged over 3months, were used for a behavior testing with an aggressive intruder. Behavioral experiments were conducted 3–4 weeks after injection of the viral expression constructs.
Wild animals	The study did not involve wild animals.
Field-collected samples	The study did not involve samples collected from the field.
Ethics oversight	All animal experiments were performed according to protocols approved by NYU and KAIST IACUC protocols for the care and use of laboratory animals. We complied with all pertinent ethical regulations.

Note that full information on the approval of the study protocol must also be provided in the manuscript.